

Direct Conversion of Methane to Methanol on $\text{LaCo}_{0.5}\text{Fe}_{0.5}\text{O}_3$ Anode in Aqueous Ionic Liquid

Zhou-Yu Su¹, Hao-Min Jiang¹, Zhi-Wei Han¹, Lu-Ting Zhang¹, Yang Tang¹, Ping-Yu Wan¹,
Zia Ul Haq Khan², Yong-Mei Chen^{1,*}

¹ College of Chemistry, Beijing University of Chemical Technology, Beijing 100029, China

² Department of Environmental Sciences COMSATS University Islamabad Vehari Campus, 61100, Pakistan

*E-mail: chenym@mail.buct.edu.cn

Received: 27 April 2022 / Accepted: 1 June 2022 / Published: 20 October 2022

The direct partial oxidation of methane (CH_4) to methanol (CH_3OH) by electrochemical method has gained considerable attention, but the percent conversion of methane, the product selectivity and the generation rate of methanol still need improvement. In this study, an electrochemical system for methane conversion is designed in which [BMIM] BF_4^- ionic liquid containing trace water ($0.2\text{-}5 \text{ mol L}^{-1}$) serve as supporting electrolyte and $\text{LaCo}_{0.5}\text{Fe}_{0.5}\text{O}_3$ as anodic catalyst for generation of active oxygen species and activation of methane. The synthesized $\text{LaCo}_{0.5}\text{Fe}_{0.5}\text{O}_3$ was confirmed by XPS to possess many oxygen vacancies in perovskite lattice, and the electrochemical study showed that certain kinds of active oxygen species could be generated through water oxidation process on $\text{LaCo}_{0.5}\text{Fe}_{0.5}\text{O}_3$ loaded electrode. CH_4 gas was bubbled near $\text{LaCo}_{0.5}\text{Fe}_{0.5}\text{O}_3$ anode in aqueous [BMIM] BF_4^- for a batch electrolysis, and CH_3OH was found in the electrolyte after electrolysis and the concentration was determined by GC-MS coupled with a headspace sampler. The results showed that the anode potential and water content in the electrolyte played vital roles during the electrochemical conversion. The formation rate of methanol of $39.3 \mu\text{mol gcat}^{-1} \text{ h}^{-1}$ with the FE of 92.4% was obtained when electrolysis in the electrolyte content 0.5 mol L^{-1} water at anodic potential of 0.8 V (vs. Ag/Ag^+), and the formation rate of $93.2 \mu\text{mol gcat}^{-1} \text{ h}^{-1}$ with the FE of 54.8% when the anodic potential was 1.0 V and the water content was 2 mol L^{-1} .

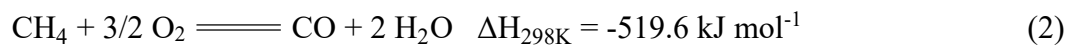
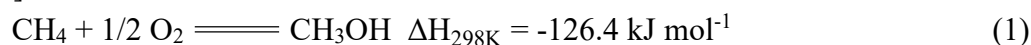
Keywords: CH_4 activation and conversion; Perovskite; Electrochemical method; Ionic liquid; Trace water

1. INTRODUCTION

Methane (CH_4) is the simplest hydrocarbon compound, exists universally in forms of natural gas, combustible ice, shale gas and marsh gas. Most methane reserves are found in remote areas such as mountains, plateaus and even oceans, making it expensive to use due to costly transport [1]. Moreover,

the potential greenhouse effect of methane is 28 times greater than that of carbon dioxide, and its influence is 84 times more potent in the past two decades [2]. Therefore, it is proposed that conversion of methane into methanol (CH_3OH) could be cost effective and aid in effective utilization of methane [3]. The state-of-the-art for methanol manufacture is a two-stage energy-extensive process, which is characterized by oxidation of methane to syngas through steam reforming, dry reforming or partial oxidative reforming technology, further followed by then catalytic reduction of syngas to produce methanol [4]. Therefore, researchers are trying to figure out a way for direct conversion of methane to methanol under mild conditions.

Theoretically, CH_4 might transform to CH_3OH by using oxygen gas as the oxidant (as shown in Reaction 1) [5]. However, methane is much more chemically inert than methanol, so the reaction of methane with oxygen is more favorable to generate CO and CO_2 instead methanol (as shown in Reactions 2 and 3) [6-7].



Direct conversion of methane to methanol means controlling partial oxidation of methane, that needs to activate C-H bond in CH_4 and avoid the peroxidation of CH_3OH simultaneously. As an accepted strategy, researchers are trying to introduce a reagent with appropriate oxidizing capacity into the system. Several forms of active oxygen species (such as superoxide radicals, peroxide anions and hydroxy radicals, et al.) have been deliberately designed by enzyme catalysis [8-12], heterogeneous catalysis [13-16], homogeneous catalysis [17-22], photocatalysis [5,23-27], or electrocatalysis systems [28,29].

In the reported electrochemical systems, active oxygen species were produced *in situ* through ORR or OER process, and then reacted with the activated methane [30]. Many theoretical calculations result confirmed some sort of relationship exists between OER and the effect of methane conversion [38,39]. However, the Faradaic efficiency (FE) is extremely low in aqueous electrochemical systems, the possible suggested reasons are the poor solubility of methane in water, the low generation rate of active oxygen species and their short lifespan in aqueous media. On contrary, catalysts for methane activation are also important. Torabi A et al. [34] used La doped SrTiO_3 as the anode in a fuel cell device operated at $300 \sim 600^\circ\text{C}$ and obtained CH_3OH in 90% selectivity in products. For an ABO_3 perovskite oxide, doping in B-site by low valence states or variable valency ion can introduce oxygen vacancy in lattice, which might improve its OER performance [35-37].

In this study, $\text{LaCo}_{0.5}\text{Fe}_{0.5}\text{O}_3$ is synthesized which possesses perovskite-type with many oxygen vacancies in lattice, and its analogues are reported to display excellent stability and performance in WOR process [41-43] and suitable features for methane activation [41,44]. The aqueous ionic liquid, that is $[\text{BMIM}] \text{BF}_4^-$ containing trace water, is prepared as supporting electrolyte. $[\text{BMIM}] \text{BF}_4^-$ is an aprotic room temperature ionic liquid, and its methane solubility is three times that of water [45]. The ionic liquid has low vapor pressure, enabling easy separation of methanol from the reaction liquid. The study idea is the trace water in ionic liquid might be catalyzed by perovskite-type oxide on anode to provide certain active oxygen species, and the Faraday efficiency is expected to be enhanced since OER process is effectively avoided and the lifespan of active oxygen species is prolonged in ionic liquid.

2. EXPERIMENTAL SECTION

2.1 Synthesis of $\text{LaCo}_{0.5}\text{Fe}_{0.5}\text{O}_3$ perovskites

$\text{LaCo}_{0.5}\text{Fe}_{0.5}\text{O}_3$ perovskites were synthesized by the hydrothermal route. The mixture of 0.002 mol $\text{La}(\text{NO}_3)_3 \cdot 6\text{H}_2\text{O}$, 0.001 mol $\text{Fe}(\text{NO}_3)_3 \cdot 9\text{H}_2\text{O}$ and 0.001 mol $\text{Co}(\text{NO}_3)_2 \cdot 6\text{H}_2\text{O}$ were dissolved in 80 mL deionized water, and then 0.004 mol citric acid and 600 mg of polyvinylpyrrolidone (PVP) are added into the above solution. After dissolution, the pH was adjusted to ~ 8.9 by $\text{NH}_3 \cdot \text{H}_2\text{O}$ solution (25.0 - 28.0 wt%). After stirring for 30 minutes, this solution was transferred into a 100 mL Teflon lining autoclave, then provided by 180 °C temperature for 24 h. After cooling down to room temperature, the mixture was filtered and washed by deionized water for three times, followed by drying at 80°C for 12 h. The solid was ground and put into a muffle furnace and heated to 700 °C at a rate of 5 °C/min and then kept under air for 3 hours, finally a brownish black powder was obtained, named $\text{LaCo}_{0.5}\text{Fe}_{0.5}\text{O}_3$. As the contrast samples, LaCoO_3 and LaFeO_3 were synthesized as the same route described above except for no addition of $\text{Fe}(\text{NO}_3)_3 \cdot 9\text{H}_2\text{O}$ or $\text{Co}(\text{NO}_3)_2 \cdot 6\text{H}_2\text{O}$.

2.2 Structural Characterization

The crystal structure was analyzed by XRD (Brucker D-8 avance) with Cu X-ray source. The measurement was performed in the scan range of $2\theta = 5^\circ - 90^\circ$ with a scan rate of $10^\circ \text{ min}^{-1}$. The surface morphology and particle size were analyzed by TEM (HITACHI H-800). The sample was dropped on a carbon-coated copper grid ($d = 2$ mm) after ultrasonic dispersion with ethanol. The morphology was analyzed by SEM (Zeiss SUPRA 55) at an accelerating voltage of 20 kV. The sample powder was directly loaded on the carbon tape of the SEM sample disk. XPS (Thermo Scientific K-Alpha+) spectra were recorded with Al Ka radiation under vacuum conditions (about $5 * 10^{-9}$ mbar). XPS spectra were obtained in CAE scanning mode with 15 kV voltage and 15 mA beam current.

2.3 Electrode preparation

Carbon paper (N030) is used as the substrate electrode. 2.4 mg of $\text{LaCo}_{0.5}\text{Fe}_{0.5}\text{O}_3$ and 200 μL 1 % Nafion solution was mixed by ultrasonic to obtain catalyst ink. The catalyst ink was loaded on the surface of carbon paper by drop-casting method. 10 μL of the same catalyst ink was dropped on the RRDE disk electrode to prepare the test electrode.

2.4 Electrolyte preparation

The supporting electrolyte was prepared by adding trace water into [BMIM]BF₄ ionic liquid, and the water contents in ionic liquid were explored from 0.1 mol L⁻¹ to 5 mol L⁻¹ in this study. Unless otherwise specified, the electrolyte mentioned hereinafter is referred to [BMIM]BF₄ solution containing 0.5 mol L⁻¹ H₂O.

2.5 Electrochemical property studies

A single-chamber electrolysis bath system was setup with three electrodes: the catalyst coated electrode (1.0 cm^2) was used as the working electrode, the Pt electrode (1.0 cm^2) was used as the counter electrode, and the self-made Ag/ Ag^+ electrode with 0.01 mol L^{-1} MeCN as the electrolyte was used as the reference electrode. CHI660E electrochemical workstation (Shanghai Chenhua Instrument Co., Ltd.) was used for testing. All measurements were performed after purging with Ar gas for at least 30 min. Cyclic voltammograms (CVs) were collected at a scan rate of 50 mV/s between -1.2 to 1.3 V. Linear sweep voltammograms (LSVs) were measured at a scan rate of 20 mV/s . Some CV and LSV tests were carried out in the RRDE system (PINE) where disk electrode serves as the working electrode with a rotating speed of 1600 rpm. For the continuous electrolysis experiment, the constant potential electrolysis mode was used, and the electrolysis was operated for 1 h.

2.6 Determination of methanol

The methanol concentration in the electrolyte was determined by a GC-MS (SHIMADZU GCMS-MP2010 SE) coupled with a headspace sampler (HS-10). The temperatures of the oven, loop, and transfer line in HS were set at 80, 100, and 120°C , respectively. The vial was heated at 80°C for 20 min without shaking, and pressurized for 3 min at 120 kPa; the loop filling and equilibration times were set at 1.50 min and 0.30 min, respectively, and the injection time was set at 1.0 min. One milliliter sample solution of each pool was placed in the HS vial. The chromatographic column was an Agilent HP-INNOWAX column ($30\text{ m} \times 0.25\text{ mm} \times 0.25\text{ }\mu\text{m}$). The injector temperature was 200°C with 10:1 split mode, and the injection volume of sample was $1\text{ }\mu\text{L}$. The high-purity He (99.999%) was used as the gas carrier, and the flow rate and pressure were 1.0 mL min^{-1} and 22.7 kPa, respectively. The ionization and the interface temperature in MS were adjusted to 230°C and 200°C . The oven temperature was programmed for 35°C for 5 min, then increased to 80°C at 5°C min^{-1} , and then to 200°C at $30^\circ\text{C min}^{-1}$ (held for 2 min). The solvent delay of 2.5 minutes. During MS detection, the selected SIM mode was chosen to reduce the interference of other organics, and the strongest fragment peak of 31 m/z was identified as the selected ion peak of methanol.

The standard curves of methanol concentration in $[\text{BMIM}] \text{BF}_4^-$ containing different water contents were established, and all the linear correlation coefficients were greater than 0.995. The Error test was executed by using two groups of standard 10 nmol mL^{-1} and 50 nmol mL^{-1} of CH_3OH solutions. The results revealed that RSD was respectively 5.77% and 2.80% and the recoveries were respectively 93.9 - 110.7% and 93.6 - 103.4%.

Based on the determined concentration of methanol (c) in the electrolyte after electrolysis, the generation rate of methanol (r) and the Faraday efficiency of generated methanol (η) are calculated as follows:

$$r (\mu\text{mol g}_{\text{cat}}^{-1} \text{ h}^{-1}) = \frac{c \cdot V_{\text{electrolyte}}}{m_{\text{cat}} \cdot t} \quad (4)$$

$$\eta (\%) = \frac{c \cdot V_{\text{electrolyte}} \cdot zF}{Q_{\text{practical}}} \times 100\% \quad (5)$$

3. RESULTS AND DISCUSSION

3.1. Structural characterization of $\text{LaCo}_{0.5}\text{Fe}_{0.5}\text{O}_3$

The TEM image of $\text{LaCo}_{0.5}\text{Fe}_{0.5}\text{O}_3$ powder (Fig. 1a) reveals that the average particle size of primary particles was $26.5 \text{ nm} \pm 7.85 \text{ nm}$, with good uniformity and slight sintering among particles. The SEM image (Fig. 1b) reveals aggregate formation with a diameter of $0.5 - 4 \mu\text{m}$ by the primary particle with loose combination. In fact, the prepared powder could be resuspended in water or organic solvent by ultrasonic concussion.

The XRD pattern of $\text{LaCo}_{0.5}\text{Fe}_{0.5}\text{O}_3$ is shown in Fig. 2. The relative peak intensity and peak position of all diffraction peaks were consistent with the standard pattern (JCPDS No. 40-0224), except for the peak near $2\theta = 26^\circ$ which belongs to the complex carbonization residue. It is interpreted that the prepared compound had perfect perovskite crystal form, that was the site A and B in perovskite oxide was partly occupied by Fe and Co atoms in good crystallinity and no other oxides co-existed.

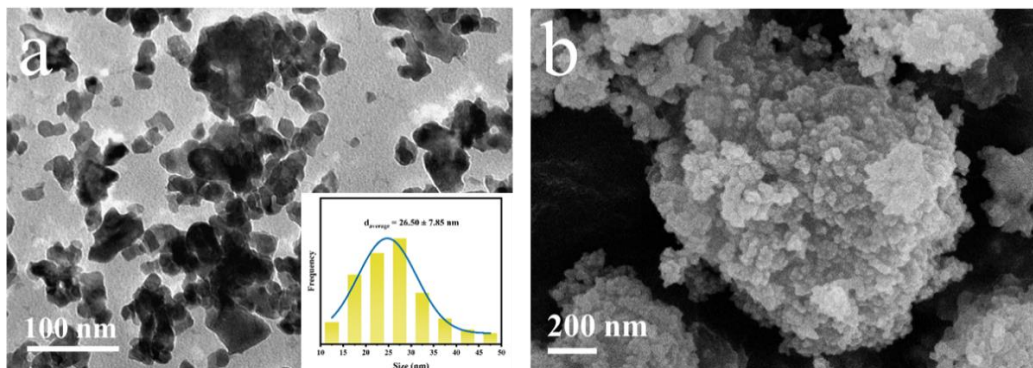


Figure 1. (a) TEM and (b) SEM images of $\text{LaCo}_{0.5}\text{Fe}_{0.5}\text{O}_3$

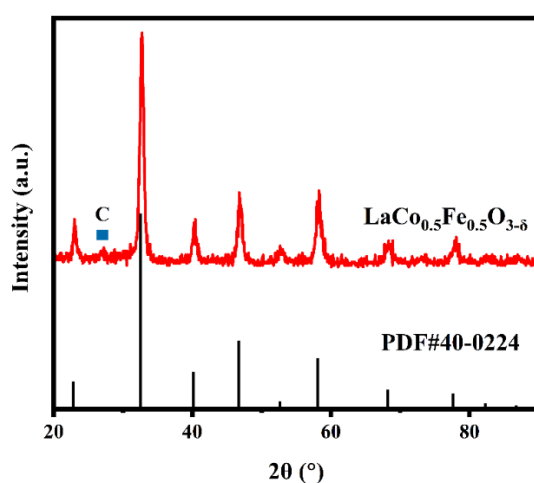


Figure 2. XRD pattern of perovskite-like catalysts $\text{LaCo}_{0.5}\text{Fe}_{0.5}\text{O}_3$ by hydrothermal method

The XPS spectra of $\text{LaCo}_{0.5}\text{Fe}_{0.5}\text{O}_3$ is shown in Fig. 3. The La 3d_{5/2} XPS spectrum (Fig. 2a) is

proof that all La ions in the sample had a single valence state of La^{3+} . The Fe 2p XPS spectrum (Fig. 2b) shows that both Fe^{2+} and Fe^{3+} existed, and the amount of Fe^{2+} cations accounted for a large fraction. The Co 2p XPS spectrum (Fig. 2c) also shows the presence of Co^{2+} and Co^{3+} , of which the amount of Co^{3+} accounted for a large fraction. The Gaussian fitting and deconvolution results of O 1s XPS spectra (Fig. 2d) disclose that O atoms existed in three sorts of chemical environment, that was the adsorbed oxygen (B.E. = 534.0 eV), the surface oxygen (B.E. = 531.9 eV) and the lattice oxygen (B.E. = 529.5 eV). Based on the peak fitting analysis results as shown in Fig. 4, it implies that many oxygen vacancies (O_v) were introduced into the lattice due to the co-doping of Fe and Co [46].

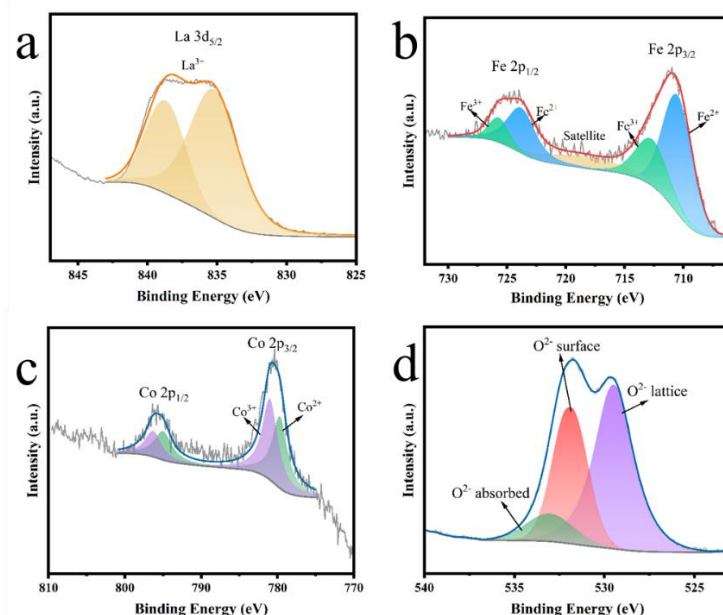


Figure 3. (a) La 3d_{5/2} (b) Fe 2p (c) Co 2p (d) O 1s XPS spectra of $\text{LaCo}_{0.5}\text{Fe}_{0.5}\text{O}_3$

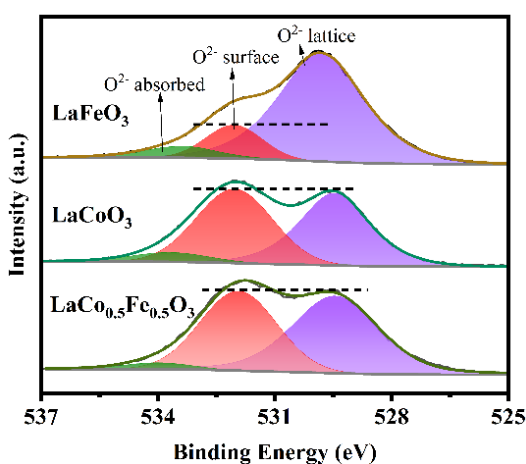


Figure 4. O 1s XPS spectra of $\text{LaCo}_{0.5}\text{Fe}_{0.5}\text{O}_3$, LaCoO_3 , LaFeO_3

3.2 Electrochemical properties of the catalysts

The CV curves of RRDE electrode loaded with $\text{LaCo}_{0.5}\text{Fe}_{0.5}\text{O}_3$ in $[\text{BMIM}]\text{BF}_4$ containing 0.5 mol/L water under Ar or CH_4 atmosphere are shown in Fig. 5a. A strong cathodic current appeared in the range of -0.75 V to -1.25 V (vs. Ag/Ag^+ , the same below), which was attributed to the hydrogen evolution process of water in the electrolyte. Moreover, the anodic current increased slowly as the potential positive-shifted from 0.2 V to 1.2 V, and it enhanced significantly when the potential was more positive than 1.2 V. The anodic current was attributed to the oxidation of water (WOR) process, while certain active oxygen species were generated and most of them adsorbed on the anode surface to become O_2 molecules before further oxidizing [2].

The CV curves (Fig. 5a) and LSV curves (Fig. 5b) under different atmospheres show that instead of the Ar atmosphere the anode current intensity was vigorous under CH_4 atmosphere. This phenomenon could be speculated that the adsorbed active oxygen species on the surface of anode might react with CH_4 molecules, which caused more electricity required to generate more active oxygen species.

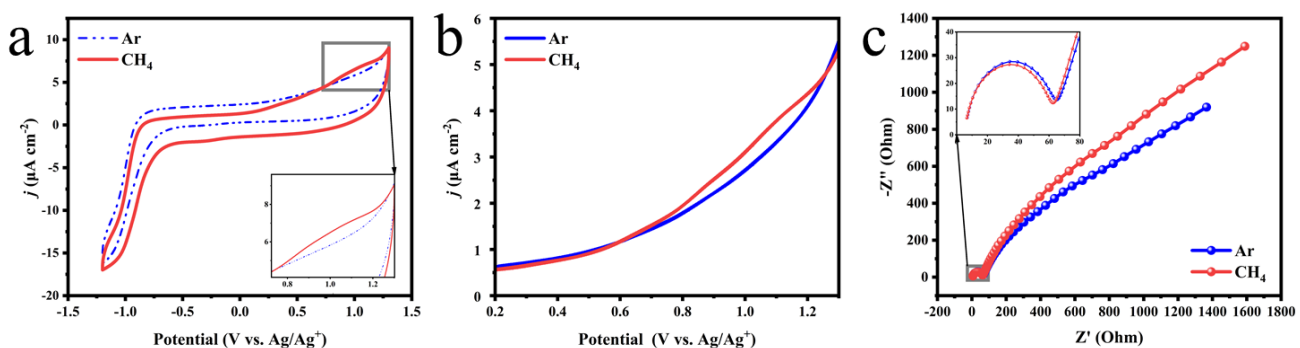


Figure 5. Comparison of (a) CV curves (b) LSV curves (c) EIS spectrum of $\text{LaCo}_{0.5}\text{Fe}_{0.5}\text{O}_3$ in Ar/ CH_4 atmospheres in $[\text{BMIM}]\text{BF}_4$ containing 0.5 mol L^{-1} water

As shown in Fig. 5c, the EIS spectrum of $\text{LaCo}_{0.5}\text{Fe}_{0.5}\text{O}_3$ electrode in $[\text{BMIM}]\text{BF}_4$ containing 0.5 mol/L water displayed a relatively perfect semicircle in the low-frequency region and a straight-line state with the abscissa of 45° in the high-frequency region, indicating that the electrode reaction process was mainly controlled by diffusion (e.g. the so-called Warburg diffusion). It is also demonstrated that CH_4 molecules might participate in the interfacial charge transfer process due to decrease in the electron transfer resistance of the redox reaction on the interface of electrode/electrolyte in the presence of CH_4 instead of the Ar atmosphere.

The comparison of CV curves of $\text{LaCo}_{0.5}\text{Fe}_{0.5}\text{O}_3$ electrode in Ar and CH_4 atmosphere in different electrolyte is shown in Fig. 6a. It shows that the current intensity originated from WOR and HER processes gradually rise as the increase in water content increased. The fact that the background current of electrolyte changed significantly as the water content changed was reasonable because adding some amount of water into $[\text{BMIM}]\text{BF}_4$ might greatly affect the viscosity and conductivity. Just for this reason, the anode current intensity in different electrolytes could not be compared with each other, but the

difference in the same electrolyte under Ar and CH₄ atmosphere could provide information about the electrochemical activity of methane. As shown in Fig. 6b-d, the difference of anode current in two atmospheres varied with different water content, and presented the maximum change when the water content was 2 mol L⁻¹ (shown as Table 1). It could be explained that the viscosity of the aqueous electrolyte system decreased and the conductivity increased as water content in ionic liquid increased, which was conducive for CH₄ molecules dissolved in electrolyte to diffuse to the anode surface for reaction. However, when the water content was too high (more than 2 mol L⁻¹), WOR reaction became more intensive, which led to reduction in the proportion of current needed to produce active oxygen in the whole anode current.

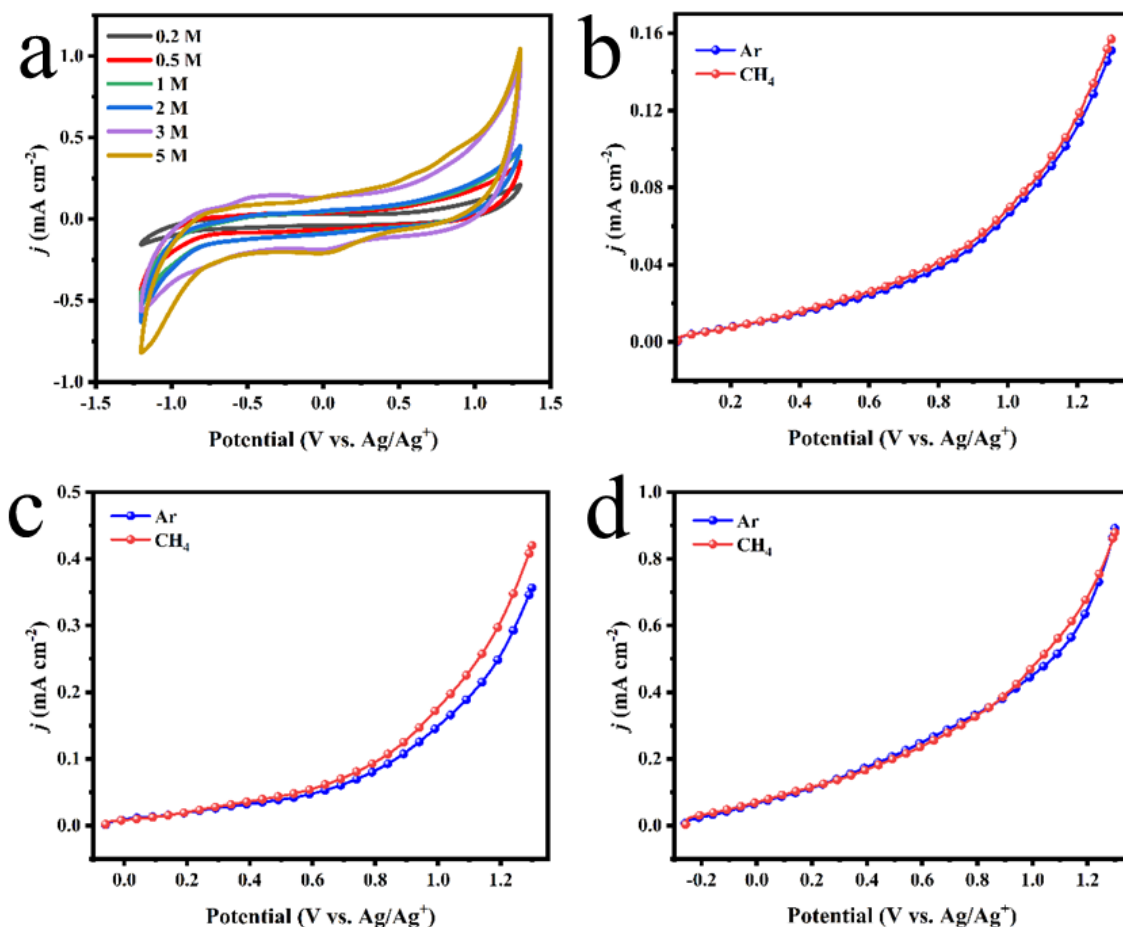


Figure 6. (a) CV curves of LaCo_{0.5}Fe_{0.5}O₃ measured under Ar atmosphere in [BMIM]BF₄ with different concentration of H₂O (b-d) LSV curves measured under Ar/CH₄ atmosphere in [BMIM]BF₄ with (b) 0.2 mol L⁻¹ (c) 2 mol L⁻¹ (d) 5 mol L⁻¹ of H₂O

3.3 Effect of electrochemical methane conversion to methanol

Electrochemical conversion of methane was conducted in a non-diaphragm electrolysis bath under CH₄ atmosphere by potentiostatic mode. The results under different electrolysis conditions are shown in Table 1.

Table 1. Continuous electrolysis results under different reaction conditions

No.	Catalysts	Potential/V	Content of H ₂ O/ (mol L ⁻¹)	<i>r</i> / ($\mu\text{mol g}_{\text{cat}}^{-1} \text{ h}^{-1}$)	$\eta/\%$
1	LaCoO ₃	1.0	0.5	42.2	43.0
2	LaFeO ₃	1.0	0.5	39.3	42.8
3	LaCo _{0.5} Fe _{0.5} O ₃	0.8	0.5	39.3	92.4
4	LaCo _{0.5} Fe _{0.5} O ₃	0.9	0.5	48.6	82.5
5	LaCo _{0.5} Fe _{0.5} O ₃	1.0	0.5	62.6	65.7
6	LaCo _{0.5} Fe _{0.5} O ₃	1.1	0.5	45.3	33.3
7	LaCo _{0.5} Fe _{0.5} O ₃	1.2	0.5	19.5	8.0
8	LaCo _{0.5} Fe _{0.5} O ₃	1.0	0.2	13.6	18.7
9	LaCo _{0.5} Fe _{0.5} O ₃	1.0	1.0	86.0	65.8
10	LaCo _{0.5} Fe _{0.5} O ₃	1.0	2.0	93.2	54.8
11	LaCo _{0.5} Fe _{0.5} O ₃	1.0	3.0	69.8	15.7
12	LaCo _{0.5} Fe _{0.5} O ₃	1.0	5.0	26.4	4.5

Different generation rate (*r*) and Faradaic efficiency (η) of methanol were obtained by using LaCo_{0.5}Fe_{0.5}O₃, LaCoO₃ and LaFeO₃ loaded anodes under the same electrolysis conditions. As shown in Entry 1, 2, and 5 in Table 1, the performance of LaCo_{0.5}Fe_{0.5}O₃ anode is the best due to its the better methane activation properties than the other catalysts [47].

Using LaCo_{0.5}Fe_{0.5}O₃ anode in the same electrolyte, the effect of anode potential on the conversion of methane was studied (Entry 3-7 in Table 1). When the anode potential was changed from 0.8 V to 1.2 V, the generation rate of methanol (*r*) firstly increased and then decreased (Fig. 7a), and the maximum rate of 59.4 $\mu\text{mol g}_{\text{cat}}^{-1} \text{ h}^{-1}$ was obtained at 1.0 V. However, the largest Faradaic efficiency (η) of 92.4% was obtained at 0.8 V, and it continuously decreased as the anode potential positive-shifted (Fig. 7b). It is reasonable that the generation rate of CH₃OH increases with the amount of the generated O* on anode, since CH₄ molecules could only be activated and converted to methanol by the generated active oxygen species [2]. And the amount of the generated O* increased in range of 0.8 V to 1.0 V, but decreased when the potential positive than 1.0 V owing to the competition of OER on anode. It was also because OER became more intensive as the anode potential positive-shifting, so that the fraction of electricity needed to generate O* to the total consuming electricity decreased gradually, resulting in the decreased FE (η).

The effect of water content in electrolyte on the methane conversion were further investigated and the results are shown in Table 1 (Entry 3 and Entry 8-12 in Table 1). The generation rate *r* increased when the water concentration changed from 0.2 mol L⁻¹ to 2.0 mol L⁻¹, and the highest *r* up to 93.2 $\mu\text{mol g}_{\text{cat}}^{-1} \text{ h}^{-1}$ and then it decreased when the water content was greater than 2.0 mol L⁻¹ (Fig. 8a). The change

of Faradaic efficiency η as the water concentration increasing was also in an inverted-V shape (Fig. 8b), and the maximum η of 65.7% was obtained in ionic liquid containing 1.0 mol L⁻¹ of water. It can be explained that the appropriate water content could lessen the viscosity and improve ionic liquid conductivity, so the mass transfer process of methane in electrolyte was improved, as well as the generation of O* through WOR on anode. However, the competition of OER would be much greater if too much water exists, committing the decrease of the FE η .

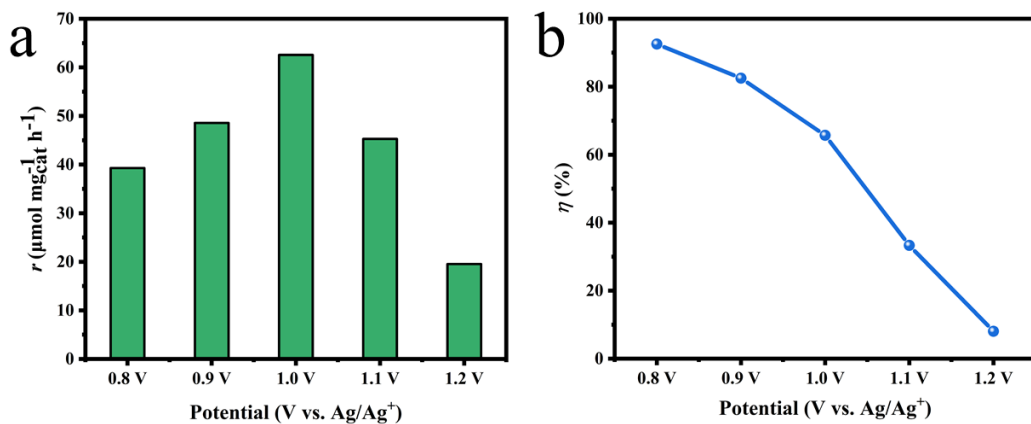


Figure 7. Continuous electrolysis results using LaCo_{0.5}Fe_{0.5}O₃ anode in [BMIM]BF₄ containing 0.5 mol/L water at different anodic potential, (a) generation rate r ; (b) Faraday efficiency η

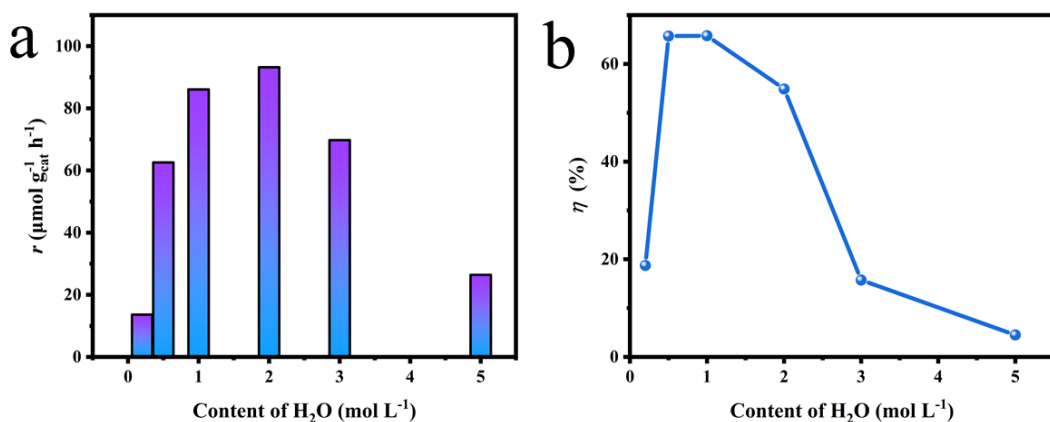


Figure 8. Continuous electrolysis results using LaCo_{0.5}Fe_{0.5}O₃ anode in [BMIM]BF₄ with different water content at 1.0V, (a) generation rate r ; (b) Faraday efficiency η

The relatively high Faradic efficiency but moderate generation rate of methanol was obtained in this work comparing with the reported studies (see the data listed in Table 2). The limited content of water in electrolyte helps to inhibit the side reaction of OER on anode, which resulted in obtaining the high Faradic efficiency. The moderate generation rate might be originated from the lagging mass transferring in ionic liquid.

Table 2. Representative studies on electrocatalytic conversion of methane to methanol

Catalyst on anode	Electrolyte	T/ (°C)	Oxygen source	CH ₃ OH generation	$\eta/\%$	Ref.
LaCo _{0.5} Fe _{0.5} O ₃	[BMIM]BF ₄ containing 0.5mol/L H ₂ O	R.T.*	H ₂ O	39.29 $\mu\text{mol g}_{\text{cat}}^{-1} \text{ h}^{-1}$	92.4	This work
TiO ₂ /RuO ₂ /V ₂ O ₅	0.1 M Na ₂ SO ₄	R.T.	H ₂ O	297 mg L ⁻¹ h ⁻¹	57	32
NiO/Ni	0.1 M NaOH	R.T.	H ₂ O	-	54	33
Cu ₂ O ₃ -TiO ₂	0.1 M K ₃ PO ₄	R.T.	H ₂ O	-	6	39
(TiO ₂ /RuO ₂)/PTFE	0.1 M Na ₂ SO ₄	R.T.	H ₂ O	74 mg L ⁻¹ h ⁻¹	30	48
V ₂ O ₅ /SnO ₂	Sn _{0.9} In _{0.1} P ₂ O ₇	100	H ₂ O	-	61.4	49

*R.T., room temperature

3.4 Electrode recycling performance

The performance of the catalyst was tested by conducting continuous electrolysis experiments for 7 hrs using the same working electrode and sampling every hour. As shown in Fig. 9, the methanol generation rate and Faraday efficiency during the test were kept relatively stable, only slight attenuation occurred.

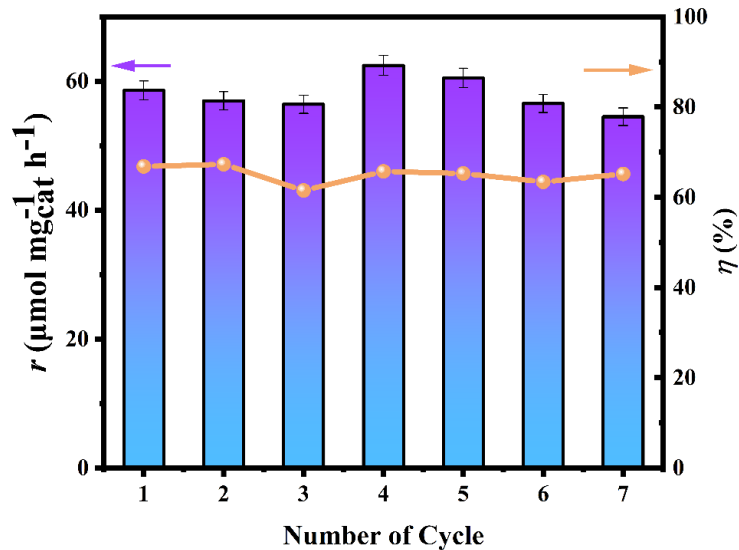


Figure 9. The continuous electrolysis by using the same LaCo_{0.5}Fe_{0.5}O₃ loaded electrode in the electrolyte of [BMIM]BF₄ containing 0.5mol L⁻¹ of water at anodic potential of 1.0 V

4. CONCLUSIONS

In this study, the direct conversion of methane to methanol at room temperature and pressure was observed in a non-diaphragm electrolytic bath where aqueous [BMIM]BF₄ served as supporting electrolyte and LaCo_{0.5}Fe_{0.5}O₃ as catalyst loaded on anode. LaCo_{0.5}Fe_{0.5}O₃ is confirmed to possess many

oxygen vacancies in perovskite lattice which attests good WOR catalytic property, so the trace water in [BMIM]BF₄ could be oxidized for generation active oxygen species (O^{*}) which adsorbed on the electrode surface. And when the dissolved CH₄ molecules in the electrolyte diffused to the anode surface and reacted with O^{*} to get converted into methanol. In this process, the generation rate of methanol r mainly depended on the generation rate of O^{*}, and the Faraday efficiency η was mainly affected by the competing OER. Therefore, it is necessary to optimize the electrolysis conditions by adjusting the anode potential and the water content in the ionic liquid. In this study, a small amount of water was added to ionic liquid to balance the contradiction between the production of reactive oxygen species and oxygen evolution process, and a better current efficiency was acquired.

ACKNOWLEDGMENTS

The authors greatly appreciate support from China National Science Foundation (No. 22075012).

References

1. J. Jang, K. Shen, C.G. Morales-Guio, *Joule*, 3 (2019) 2589.
2. J.A. Arminio-Ravelo, M. Escudero-Escribano, *Curr. Opin. Green Sustainable Chem.*, 30 (2021) 100489.
3. M.S. Alias, S.K. Kamarudin, A.M. Zainoodin, M.S. Masdar, *Int. J. Hydrogen Energy*, 45 (2020) 19620.
4. M.J. da Silva, *Fuel Process. Technol.*, 145 (2016) 42.
5. L. Luo, J. Luo, H. Li, F. Ren, Y. Zhang, A. Liu, W.-X. Li, J. Zeng, *Nat. Commun.*, 12 (2021) 1218.
6. V.C.C. Wang, S. Maji, P.P.Y. Chen, H.K. Lee, S.S.F. Yu, S.I. Chan, *Chem. Rev.*, 117 (2017) 8574.
7. I. Bar-Nahum, A.M. Khenkin, R. Neumann, *J. Am. Chem. Soc.*, 126 (2004) 10236.
8. R. Whittenbury, K.C. Phillips, J.F. Wilkinson, *Microbiology*, 61 (1970) 205.
9. A. Gilman, L.M. Laurens, A.W. Puri, F. Chu, P.T. Pienkos, M.E. Lidstrom, *Microb. Cell Fact.*, 14 (2015) 182.
10. R. Banerjee, Y. Proshlyakov, J.D. Lipscomb, D.A. Proshlyakov, *Nature*, 518 (2015) 431.
11. H.J. Kim, J. Huh, Y.W. Kwon, D. Park, Y. Yu, Y.E. Jang, B. R. Lee, E. Jo, E.J. Lee, Y. Heo, W. Lee, J. Lee, *Nat. Catal.*, 2 (2019) 342.
12. C.C. Liu, T.S. Lin, S.I. Chan, C. Y. Mou, *J. Catal.*, 322 (2015) 139.
13. P.E.E. James E.Lyons, Vincent A.Durante, *Stud. Surf. Sci. Catal.*, 67 (1991) 99.
14. M.V. Parfenov, E.V. Starokon, L.V. Pirutko, G.I. Panov, *J. Catal.*, 318 (2014) 14.
15. Z. Jin, L. Wang, E. Zuidema, K. Mondal, M. Zhang, J. Zhang, C. Wang, X. Meng, H. Yang, C. Mesters, F. S. Xiao, *Science*, 367 (2020) 193.
16. T. Yu, Z. Li, L. Lin, S. Chu, Y. Su, W. Song, A. Wang, B.M. Weckhuysen, W. Luo, *ACS Catal.*, 11 (2021) 6684.
17. M. Ravi, M. Ranocchiari, J.A. van Bokhoven, *Angew. Chem., Int. Ed.*, 56 (2017) 16464.
18. H.T. Dang, H.W. Lee, J. Lee, H. Choo, S.H. Hong, M. Cheong, H. Lee, *ACS Catal.*, 8 (2018) 11854.
19. R. Palkovits, C. von Malotki, M. Baumgarten, K. Müllen, C. Baltes, M. Antonietti, P. Kuhn, J. Weber, A. Thomas, F. Schüth, *ChemSusChem*, 3 (2010) 277.
20. T. Zimmermann, M. Soorholtz, M. Bilke, F. Schüth, *J. Am. Chem. Soc.*, 138 (2016) 12395.
21. L.C. Kao, A.C. Hutson, A. Sen, *J. Am. Chem. Soc.*, 113 (1991) 700.
22. I.P.S.a.I.I.M. M. N. Vargaftik, Journal of the Chemical Society, *Chem. Commun.*, 15 (1990) 1049.
23. L.J. Zhang, S. Li, B.K. Liu, D.J. Wang, T.F. Xie, *ACS Catal.*, 4 (2014) 3724.
24. S. Wang, L. Wang, W. Huang, *J. Mater. Chem. A*, 8 (2020) 24307.
25. Y. Zeng, H.C. Liu, J.S. Wang, X.Y. Wu, S.L. Wang, *Catal. Sci. Technol.*, 10 (2020) 2329.

26. W. Zhou, X. Qiu, Y. Jiang, Y. Fan, S. Wei, D. Han, L. Niu, Z. Tang, *J. Mater. Chem. A*, 8 (2020) 13277.
27. F. Sastre, V. Fornés, A. Corma, H. García, *J. Am. Chem. Soc.*, 133 (2011) 17257.
28. M.J. Boyd, A.A. Latimer, C.F. Dickens, A.C. Nielander, C. Hahn, J.K. Nørskov, D.C. Higgins, T.F. Jaramillo, *ACS Catal.*, 9 (2019) 7578.
29. C. Panaritis, Y.M. Hajar, L. Treps, C. Michel, E.A. Baranova, S.N. Steinmann, *J. Phys. Chem. Lett.*, 11 (2020) 6976.
30. A.G. Abdelkader Mohamed, S.A. Zahra Naqviab, Y. Wang, *ChemCatChem*, 13 (2021) 787.
31. S. Xie, S. Lin, Q. Zhang, Z. Tian, Y. Wang, *J. Energy Chem.*, 27 (2018) 1629.
32. R.S. Rocha, R.M. Reis, M.R.V. Lanza, R. Bertazzoli, *Electrochim. Acta*, 87 (2013) 606.
33. Z. Guo, W. Chen, Y. Song, X. Dong, G. Li, W. Wei, Y. Sun, *Chin. J. Catal.*, 41 (2020) 1067.
34. A. Torabi, J. Barton, C. Willman, H. Ghezel-Ayagh, N. Li, A. Poozhikunnath, R. Maric, O.A. Marina, *ECS Trans.*, 72 (2016) 193.
35. J. Kim, X. Chen, P.-C. Shih, H. Yang, *ACS Sustainable Chem. Eng.*, 5 (2017) 10910.
36. A. Vignesh, M. Prabu, S. Shanmugam, *ACS Appl. Mater. Interfaces*, 8 (2016) 6019.
37. T.X. Nguyen, Y.-C. Liao, C.-C. Lin, Y.-H. Su, J.-M. Ting, *Adv. Funct. Mater.*, 31 (2021) 2101632.
38. L. Arnarson, P.S. Schmidt, M. Pandey, A. Bagger, K.S. Thygesen, I.E.L. Stephens, J. Rossmeisl, *Phys. Chem. Chem. Phys.*, 20 (2018) 11152.
39. A. Prajapati, A. Collins Brianna, D. Goodpaster Jason, R. Singh Meenesh, *Proc. Natl. Acad. Sci.*, 118 (2021) e2023233118.
40. S. Yamamoto, J.B. Alcauskas, T.E. Crozier, *J. Chem. Eng. Data*, 21 (1976) 78.
41. H.C. Fonseca, N. Bion, F. Epron, D. Ruiz, S.G. Marchetti, J.F. Bengoa, M. do Carmo Rangel, *Catal. Today*, 344 (2020) 212.
42. B.-J. Kim, E. Fabbri, D.F. Abbott, X. Cheng, A.H. Clark, M. Nachtegaal, M. Borlaf, I.E. Castelli, T. Graule, T.J. Schmidt, *J. Am. Chem. Soc.*, 141 (2019) 5231.
43. B. Alkan, D. Medina, J. Landers, M. Heidemann, U. Hagemann, S. Salamon, C. Andronescu, H. Wende, C. Schulz, W. Schuhmann, H. Wiggers, *ChemElectroChem*, 7 (2020) 2564.
44. K.T.C. Roseno, R. Brackmann, M.A. da Silva, M. Schmal, *Int. J. Hydrogen Energy*, 41 (2016) 18178.
45. Y. Chen, F. Mutelet, J.-N. Jaubert, *Fluid Phase Equilib.*, 372 (2014) 26.
46. J. Jing, M.N. Pervez, P. Sun, C. Cao, B. Li, V. Naddeo, W. Jin, Y. Zhao, *Sci. Total Environ.*, 801 (2021) 149490.
47. H.S. Lim, M. Lee, D. Kang, J.W. Lee, *Int. J. Hydrogen Energy*, 43 (2018) 20580
48. R.S. Rocha, L.M. Camargo, M.R.V. Lanza, R. Bertazzoli, *Electrocatalysis*, 1 (2010) 224.
49. B. Lee, T. Hibino, *J. Catal.*, 279 (2011) 233.